Climatological Estimation of Environmental Uncertainty over the Middle Atlantic Bight Shelf and Slope

Christopher A. Linder and Glen G. Gawarkiewicz

Woods Hole Oceanographic Institution

Woods Hole, Massachusetts 02543 USA

Maureen Taylor

Northeast Fisheries Science Center

National Marine Fisheries Service

Woods Hole, Massachusetts 02543 USA

Submitted to IEEE Journal of Oceanic Engineering

June 2004

Abstract

Historical hydrographic data are used to determine the spatial and seasonal patterns of uncertainty in thermohaline and sound speed fields in a well-sampled region, the continental shelf and slope in the Middle Atlantic Bight. Several different historical databases are combined to produce two-dimensional plan view and cross-shelf fields of temperature, salinity, and sound speed in two separate regions, the New England shelf and the shelf off New Jersey and Maryland. In addition, spatial maps of the sound speed fields reveal that the maximum variance of the sound speed occurs at the edge of the continental shelf, in the vicinity of the shelfbreak front. The standard deviation of the sound speed was largest during the spring and summer, with magnitudes as large as 14 m/s in a narrow band coinciding with the mean position of the shelfbreak front. During spring the peak in variance was located near the surface outcrop of the front, but during summer the maximum variance was centered at a depth of 30 m, immediately beneath the seasonal thermocline. Comparisons with both synoptic measurements from the Shelfbreak PRIMER experiment as well as moored time series from the Nantucket Shoals Flux Experiment confirm that the shelfbreak front is a "hotspot" of uncertainty (maximum variance), and that the vertical structure of the peak variance is dependent on the presence or absence of the seasonal thermocline.

1. Introduction

The fundamental problem of characterizing uncertainty in acoustic propagation and transmission loss in shallow water is difficult because it involves both oceanographic processes within the water column as well as geoacoustic properties of the underlying ocean bottom. Furthermore, in shallow water, spatial and temporal correlation scales are often shorter than the deep ocean, so the water column is subject to substantial range dependence on a variety of scales.

While substantial interest has been devoted to internal waves and their effects on propagation for short time scales (e.g. Zhou, 1984; Duda and Preisig, 1999; Chiu et al., 2004), mid-latitude continental shelves also contain significant variability on seasonal time scales as well as mesoscale and regional spatial scales.

As part of a larger group effort to characterize regional "domains" of uncertainty, we have updated a previous climatology of the Middle Atlantic Bight (Linder and Gawarkiewicz, 1998) with improved methodology to examine the continental shelf and slope as a whole within the Middle Atlantic Bight. In addition to the cross-shelf sections produced previously, we also analyzed horizontal maps of both mean fields and variance of the temperature, salinity, and sound speed fields to allow for regional comparisons as well as a more detailed comparison with topographic features such as canyons.

The water masses of the continental shelf and slope have been described by Wright and Parker (1976). The two primary water masses in the MAB are cool, fresh shelf water and comparatively warm and saline slope water (the upper slope pycnostad, as defined by Wright and Parker (1976). The boundary between these water masses is the shelfbreak front, which contains a frontal water mass intermediate in salinity between the shelf and slope water masses (Lentz et al., 2003). Temporal evolution of the shelf water mass over an annual cycle, including the formation and evolution of the "cold pool", the winter-cooled water over the shelf, has been described by Houghton et al. (1982). Observations of the annual cycle of stratification have been presented in

Beardsley et al. (1985), Lentz et al. (2003), and Beardsley et al. (2003). Inter-annual variability of the shelf water mass including variations in fresh water content over the shelf has been examined by Mountain (2003).

A number of previous studies have quantified the mean structure and variability of the Middle Atlantic Bight shelfbreak front (Wright, 1976; Halliwell and Mooers, 1979; Naimie et al., 1994; Linder and Gawarkiewicz, 1998). In a previous study (Linder and Gawarkiewicz, 1998; hereafter, LG98) we studied the cross-shelf thermohaline structure in three distinct regions along the continental margin: the south flank of Georges Bank, the New England shelf, and the New Jersey/Maryland shelf. In this study we examine plan view maps of temperature, salinity, and sound speed from Georges Bank to Cape Hatteras. This enables us to directly compare the spatial structure of the variance of the sound speed over both the continental shelf and slope. The cross-shelf sections from the New England shelf and New Jersey/Maryland shelf are constructed with a new methodology so that the continental shelf region is resolved (depth-bin averaging in LG98 tended to clump much of the shelf structure together, distorting the cross-shelf gradients).

The organization is as follows. In section 2 we describe the data sets used in the analysis along with the methodology. The thermohaline and sound speed fields are presented in section 3 for the New England and New Jersey/Maryland shelves. In section 4, the cross-shelf variance fields are compared with recent high-resolution synoptic sections and mooring array time series. In section 5 the results are discussed including a classification of physical processes contributing to

sound speed variance on a variety of subtidal time scales. The generality of the results to other continental shelf and slope regions are also considered, along with comments on oceanographic contributions to defining "hotspots" of uncertainty in acoustic propagation and transmission loss. The results are briefly summarized in section 6.

2. Data and Methods

2.1 Data sources

The plan view climatology encompasses the entire Middle Atlantic Bight continental shelf and slope region from Georges Bank to Cape Hatteras (35-42N, 65-77W, see shaded area in Figure 1). The primary data source is *Hydrobase2* (Curry, 2002). *Hydrobase2* incorporates raw profile data from the *World Ocean Database 1998* (Levitus et al. 1998), World Ocean Circulation Experiment (WOCE) Hydrographic Programme, International Council for the Exploration of the Sea (ICES), Barents and Kara Seas Oceanographic Database (BarKode) and various other sources. In addition, we have added data from the National Marine Fisheries Service (NMFS) (collected and quality-controlled by M. Taylor) and the Shelf-Edge Exchange Processes (SEEP) program (Biscaye et al., 1994) kindly provided by C. Flagg. These datasets have been decimated to match the vertical resolution of the *Hydrobase2* data (standard bottle depths). After excluding shallow (less than 30m) and deep (greater than 3000m) stations, the total number of CTD casts per dataset are: Hydrobase2—21,835, NOAA—19,200, and SEEP—310. Of these total 41,345 stations, 30% are

from the spring (April 1 to June 30), 24% are from summer (July 1 to September 30), 20% are from autumn (October 1 to December 31), and 26% are from winter (January 1 to March 31). The majority of stations were collected during the 1990-2002 time period, although there are no over-represented years within that time period.

2.2 Methods

The seasonal plan view fields are constructed using a spatial weighted averaging scheme. Data are first binned by season (defined in section 2.1) and depth range. We will present figures from a mid-depth layer (40-55m), but near-surface (5-15m) and shelfbreak (80-100m) bins were also computed and will be discussed. Figure 2a is a sample of the output grid nodes. This shows both the resolution (0.2° in both latitude and longitude, roughly 20km spacing) and the range over which profiles are collected (25km). The temperature and salinity data points are then averaged for each grid node using a Hamming weighting function, depicted in Figure 2b. Standard deviation of the temperature and salinity is computed in a similar fashion for each node. Since we are focusing on the outer continental shelf and slope, we exclude station data shallower than 30m and deeper than 3000m. Nodes with fewer than 10 points comprising a mean are also rejected.

The data density for the mid-depth bin, broken down by season, is shown in Figure 3. The most vertical profiles are from the Georges Bank region east of the Nantucket Shoals study area, while the fewest are offshore of the 2000m isobath throughout the MAB. The profiles are

distributed relatively evenly by season with the exception of fall, where the data density is much lower from New Jersey to Cape Hatteras.

In addition to the plan view fields, we have also computed two dimensional cross-shelf fields. LG98 constructed a cross-shelf climatology of the shelfbreak front using a depth-bin averaging method. This method collapsed individual station profiles within a specified longitude band onto a single cross-shelf section. While this produced satisfactory results for regions of moderately varying bottom slope, it tended to group together profiles in somewhat unrealistic fashion for areas of weak bottom slope (i.e. on the shelf). The sections presented in this paper for the Nantucket Shoals (39-41°N, 69-72°W) and New Jersey (37-39.5°N, 72.5-75.5°W) study areas use a different mapping. Instead of using depth bins, the individual profiles are remapped according to cross-shelf distance from the 100m isobath. The 100m isobath was chosen as the reference because it roughly corresponds to the mean position of the foot of the shelfbreak front south of New England. The bins are 10km wide in cross-shelf distance and 10m deep, doubling our horizontal resolution on the shelf. Mean and standard deviation are calculated on the data in the bins with no weighting. Roughly 40% more data was present in the National Ocean Data Center (NODC) archive than was available for LG98. The new climatology also uses four three-month seasons (starting with winter, defined as Jan-Feb-Mar) instead of the bimonthly periods of LG98 in order to increase data density. All of these factors combine to greatly improve seasonal fields over the continental shelf and slope in this region.

3. Regional Patterns

3.1 Temperature

The seasonal cycle of temperature at 40-55 m appears in Figure 4. Minimum shelf temperatures range from 6 degrees C in winter and spring to 16 degrees C over the outer continental shelf during summer and fall. The largest cross-shelf gradients occur near the 100 m isobath, and correspond to the position of the shelfbreak front. Over the continental slope, temperatures are as high as 16 degrees C during summer and fall. This indicates warming at this level from the overlying surface layer, as the temperature of the upper slope pycnostad is generally 12 degrees C (Wright and Parker, 1976). Cross-shelf thermal gradients are particularly strong during the spring throughout the Middle Atlantic Bight and the summer off the New Jersey/Maryland shelf.

Two interesting areas of alongshelf thermal gradients also appear within the climatology. In every season except fall, there is a temperature difference of 2-4 degrees C between shelf water north of 37 degrees 30 minutes and shelf water south of this latitude. This presumably represents a combination of increasing solar insolation further south along with enhanced onshore heat transport due to proximity to the Gulf Stream and associated features. A second region of alongshelf gradients occurs south of the eastern tip of Long Island during the summer months. This is most

likely due to alongshelf variations in tidal mixing, as observations from the FRONTS experiment (Bogden and O'Donnell, 1997) indicate that there are tidal mixing fronts in this vicinity.

3.2 Salinity

The mid-depth mean salinity is shown in Figure 5. In contrast to the temperature, the salinity exhibits much less seasonal variation. Mountain (2003) observed that the volume and salinity of shelf water was dependent upon inputs from the Gulf of Maine, and exhibited large interannual variability. Figure 5 does show a slight freshening from Georges Bank to New Jersey for the summer season, which disappears in fall. As discussed earlier in LG98, this is presumably due to the seasonal influx of fresh water through the Middle Atlantic Bight which has advected down from the St. Lawrence River. LG98 showed that the maximum offshore extent of the foot of the shelfbreak front corresponded to the autumn, which is not when local runoff is at a maximum. They thus concluded that seasonal timing of fresh water pulses from further upstream was the most likely cause of the downstream progression and phasing of minimum salinities over the shelf. Nevertheless, as Mountain (2003) has shown, the interannual variability of the freshwater content over the continental shelf is greater than the seasonal cycle.

The plan view maps clearly show the proximity of the 34.5 isohaline that defines the core of the front to the bathymetry throughout the Middle Atlantic Bight. The front is slightly offshore of the 100m isobath at mid-depth (40-55 m) since the foot of the front, or intersection point with the

bottom, is at 100 meters south of New England. The primary mid-depth gradient is approximately 20 km seaward of the foot of the front, since the front slopes at a shallow angle (3°) upward from the foot. The maximum variance of the salinity field is at the mean position of the front (Figure 6). Since the front meanders energetically along its entire length from Georges Bank to Cape Hatteras and is known to be strongly unstable from theoretical considerations (Lozier et al., 2002), we would expect to see a maximum in variability coincident with the mean position of the front. Salinity standard deviation maximums are clearly observed in Figure 6 just seaward of the 100m isobath throughout the year. The seasonal distribution of these maximums is interesting. The south flank of Georges Bank shows up as the area with largest variance for all seasons. One possible explanation for the high standard deviation of temperature along the south flank of Georges Bank is the presence of warm core rings. Westward drift of warm core rings might result in their being detained for longer periods of time near the shelfbreak as they encounter the south flank, which has a more northeasterly orientation. Further west, south of New England, the orientation of the shelfbreak does not prevent westward motion. Spring and summer are also clearly more variable than fall and winter. This is most likely due to the seasonality of fresh water inputs locally from the Gulf of Maine. We have also computed these statistics for near-surface (5-15m) and shelfbreak (80-100m) depth bins. The near-surface salinity standard deviation exhibits a much greater cross-shelf extent, presumably due to wind-forced motions of the surface mixed

layer. The cross-shelf extent of the standard deviation is a narrow band in the 80-100m bin, centered on the shelfbreak front.

3.3 Sound speed

Since sound speed is dominated by water temperature, the mean sound speed (Figure 7) closely resembles the mean temperature map. The combination of temperature and salinity gradients produces a large mid-depth cross-frontal sound speed gradient. The slowest sound speed is located in the cold pool, the winter-cooled shelf water beneath the seasonal pycnocline. The highest sound speeds are found in the warm slope water. The gradient is a maximum (order 40 m s^{-1}) during winter and spring, subsiding to 20 m s^{-1} during the fall transition season when mixing breaks down the seasonal thermocline. Figure 8 shows sound speed standard deviation. Note that the cross-shelf extent of the sound speed variance is actually larger than that of the variance for either temperature or salinity. This implies that the salinity gradients, which are not exactly coincident in the cross-shelf with the temperature gradients, also contribute to the variance of the sound speed.

4. Cross-shelf fields for Nantucket Shoals

Two-dimensional cross-shelf fields for two study areas, Nantucket Shoals and New Jersey, have also been computed (study areas shown in Figure 1). The bounds of the Nantucket Shoals area are 39-41°N, 69-72°W.

4.1 Temperature

Figure 9 shows the Nantucket Shoals mean (color contours) and standard deviation (black line contours) of temperature. In winter, the shelf is isothermal. The maximum variance occurs in the heart of the front, centered at a depth of 50-80m. The magnitude of the amplitude, 2.5 degrees C, is small. In spring, as insolation increases, higher standard deviations are observed at the surface. The peak value for the standard deviation is much larger, 4 degrees C, and is concentrated in the upper 20 m of the water column. The summer season is a perfect canonical picture of shelfbreak frontal temperature and variation. The seasonal thermocline is well developed, extending to 30m depth. The variability maximum is a subsurface maximum, immediately beneath the seasonal thermocline (35-40 m depth). The vertical position is most likely determined by the baroclinic instability of the front. A linear stability analysis of the summer configuration of the front (Gawarkiewicz, 1991) indicates that the most unstable mode of the front consists of pycnocline-trapped motions. The maximum cross-shelf motion of the front occurs in the stability model, immediately beneath the seasonal thermocline, consistent with the vertical structure of the variance. During summer, the peak standard deviation occurs, with a maximum of 5 degrees C.

The thermal structure during the fall is the most unusual. Storm-driven mixing tends to vertically homogenize the thermal field and destroy the seasonal pycnocline. Temperatures over the continental shelf are the warmest (13 degrees C). The peak in variance within the water column is again surface-trapped, with a maximum standard deviation of 4 degrees C. However, the vertical extent of the local maximum is 40 m, double that of the spring.

4.2 Salinity

The seasonal salinity fields exhibit much less seasonal variation (Figure 10). The structure of the standard deviation field is broadly similar in winter, summer, and fall, with a surface-trapped maximum of 0.75 to 1.0 PSU near the surface expression of the front. However, spring is extremely different. The spring freshet and associated offshore wind-driven transport (e.g. Lentz et al., 2003) results in a significant increase in the magnitude of the standard deviation, to 4.5 PSU. There is a broadly distributed surface maximum of 3 PSU which extends to the 100 m isobath, and is concentrated in the upper 25 m of the water column. At the shelfbreak, there is still a local maximum, but it merges more smoothly into the surface-trapped maximum from the mid-shelf region.

4.3 Sound speed

Because of the large gradients in both temperature and salinity, the shelfbreak frontal region is an area of extremely large gradients in sound speed (Figure 11). In winter, 30 m s^{-1} gradients across the front exist over a span of only 20km. A peak in variability is seen at mid-depth (50-60m) in the maximum gradient region. It is likely that another peak exists at cross-shelf distances greater than 40 km, but there are not a sufficiently large number of stations offshore.

The maximum magnitude of the standard deviation in spring is surface-trapped, and has a magnitude of 14 m s^{-1}. The surface thermal gradient region in spring occurs within 40 km of the shelfbreak, and thus is properly resolved, in contrast to the winter. In summer, the peak values in standard deviation occur within the sub-surface front at a depth of 30-40 m, consistent with the thermal field discussed earlier. The cross-shelf structure of the variance field of sound speed in fall also is quite similar to that of the thermal field.

5. Cross-shelf fields for New Jersey

The New Jersey study area (shown in Figure 1) is defined by the box 37-39.5°N, 72.5-75.5°W.

5.1 Temperature

Figure 12 shows the mean and standard deviation of temperature for the New Jersey study area. The results are similar to the Nantucket Shoals study area. In winter, the shelf is nearly

isothermal, and the maximum standard deviation is surface-trapped with a maximum value of 3.5 degrees C at the offshore edge of the section. During spring, the maximum standard deviation is strongly surface trapped and is not confined to the frontal zone. As will be seen in the salinity field, this is most likely due to the influence of buoyant estuarine plumes. During summer and fall, the cross-shelf structure of the standard deviation field is again similar to Nantucket Shoals. The maximum standard deviation in summer is immediately beneath the seasonal thermocline and is confined to the frontal region. The maximum is slightly larger than for Nantucket Shoals (5 versus 4.5 degrees C).

5.2 Salinity

The salinity fields are again similar to Nantucket Shoals for winter, summer and fall. The significant difference, as in temperature, is during the spring. The variance maximum is surface-trapped, and is relatively constant from mid-shelf (x=-60 in Figure 13) out to the shelfbreak front (x=20 km). The maximum standard deviation is 4.75 PSU, which is significantly larger than Nantucket Shoals. Spring is the time of maximum run-off for both the Delaware and Hudson Rivers, both of which are associated with significant buoyant plumes. The presence of the buoyant plume increases the variance of the salinity field across the entire outer shelf over the upper 20 m of the water column.

5.3 Sound speed

The sound speed fields off New Jersey appear in Figure 14. The cross-shelf structure of the variance field is again similar to Nantucket Shoals in winter, summer, and fall. The sub-surface maximum during summer is slightly larger than Nantucket Shoals (16 versus 14 m s^{-1}). During spring, the maximum standard deviation is surface-trapped, but has a local maximum that is well shoreward of the shelfbreak (x=-40 km in Figure 14). The maximum is the largest in either region for any season, 18 m s^{-1}. Thus the presence of the buoyant plumes in this region has a significant effect on the cross-shelf structure of the variance of the sound speed, salinity, and temperature fields.

6. Other Temporal Statistics for Temperature

6.1 Temperature distributions across the shelf and slope

Another means of considering uncertainty is to examine the probability of different temperatures at a single spot throughout the year. We now present two temperature records collected during the Nantucket Shoals Flux experiment (Beardsley et al., 1985). The thermistors were located at depths of 28 m over the outer shelf (90 m depth) and at 32 m over the upper slope (400 m depth). The two instruments thus straddle the shelfbreak front. Figure 15 shows histograms of temperature from the shelf (a-d) and slope (e-h) by season. During the winter, there is a sharp peak in the probability density function at 4.5 to 5 degrees C. This is presumably the dominant

cold pool water mass formed during the winter. However, there is a range from 2 to 10 degrees C. This distribution is roughly Gaussian. Over the slope during winter, the distribution is more nearly bimodal, with peaks at 8 and 12 degrees C. There is a much broader range of temperatures than over the shelf (5 to 16 degrees C), which presumably is due to warm surface slope water. During spring, the shelf temperatures are concentrated in a band between 4 and 8 degrees C. The slope temperature ranges from 5 to 21 degrees C due to the proximity of Gulf Stream water associated with a warm core ring. (During the year long record, ten different warm core rings passed through the vicinity of the array). Note that there is now a maximum probability at 15 degrees C, and the distribution is not bimodal.

During summer, the modal temperatures over the shelf and slope are 10 and 20 degrees C, respectively. The distributions appear to be crudely similar to a chi-square distribution, but are mirror images due to their relative positions over the shelf and slope. The range of temperature over the shelf is largest during summer, with temperatures ranging from 7 to 20 degrees C. The warmest modal temperature is during fall, when the most likely temperature is 14.5 degrees C. The modal temperature over the slope is only slightly warmer, at 17 degrees C. In summary, the probability density functions of temperature differ greatly across the front, and the seasonality also affects the modal temperature, the range, and the shape of the probability density function of the temperature.

6.2 Temporal Evolution of Temperature and Stratification

A limitation of discussing the seasonal evolution is the large averaging time (3 months) used to produce the climatology. We now examine the monthly evolution of near-surface thermal structure and stratification. A simple means of quantifying the surface thermal stratification is the difference between temperature at 5 m and 20 m. The breakdown by month for both the shelf and slope (only using the NMFS data) is shown in Figure 16. The largest mean difference is during July, when the temperature difference is 5 degrees C. During winter, the difference is nearly zero. It is interesting that the scatter of points is not large during the spring transition, with maximum values of temperature difference being on order of 5 degrees C. During August, September, and October, there is a huge range of temperature differences, of 15 degrees C or greater. This is presumbably related to the timing of the breakdown in stratification due to storms and strong wind mixing energy (e.g. Lentz et al., 2003). It is interesting to note that even though the mean temperature difference is quite small in October, there is a huge range, in contrast to summer, when both the mean and the maximum difference are both substantial.

The stratification cycle over the shelf and slope is dominated by the seasonal cycle, as one would anticipate. Figure 16b shows the mean of the maximum Brunt-Vaiasala frequency by month, along with the spread of the individual data. The maximum stratification is strongest in July, with a value of 0.005 s^{-1}. The scatter is large in the summer and fall. April also has a large range, which may reflect the influence of low salinity buoyant plumes. The monthly distribution of

the depth of the maximum stratification is also shown (Figure 16c). The depth of the peak stratification is at 10 m depth in July, dropping to 40 m in February. It is interesting to see values as large as 150 m in the range of the data during winter.

6.3 Synoptic Uncertainty from the Shelfbreak PRIMER Experiment

It is important to consider whether short-term, synoptic measurements yield a cross-shelf distribution of variance which is similar to that of the seasonal climatology. We use the observations collected during the summer Shelfbreak PRIMER experiment to examine this question.

During the Shelfbreak PRIMER experiment, observations were collected using the WHOI (Woods Hole Oceanographic Institution) SeaSoar, a towed undulating vehicle. The horizontal resolution of the processed data was 1 km and the vertical resolution 2 m. Details of the processing and spatial maps of the thermohaline and velocity fields appear in Gawarkiewicz et al. (2004). The sampled grid consisting of four cross-shelf transects was repeated at one day intervals for six days. The sampling resolved both the spatial and temporal correlation scales so that statistically significant three-dimensional maps of the fields could be constructed for a 30 km (alongshelf) by 50 km (cross-shelf) domain.

The mean temperature field from the westernmost cross-shelf section from PRIMER, along 71^{o} 10' W, appears in Figure 17. The two primary features of summer hydrography, the strong

seasonal thermocline and the winter-cooled shelf water, the "cold pool", are apparent. The offshore edge of the cool shelf water is the shelfbreak front. Since we have six separate sections along this line, we can use Empirical Orthogonal Function (EOF) analysis to examine the modal structures. The dominant mode, which accounts for 43% of the variance, shows an offshore maximum at the point at which the sub-surface shelfbreak front intersects the seasonal thermocline (Figure 18a). The offshore extent of this extremum is not resolved, but it is likely to be bounded by the maximum offshore displacement of the front. The second mode (Figure 18b) accounts for 28% of the variance. The maximum amplitude for this mode is in the middle of the front, and is associated with vertical displacement of the seasonal thermocline. The third mode (not shown) has a maximum at the foot of the front, where the frontal isotherms intersect the bottom, and significant amplitudes along the front at mid-depth. Thus, even for shorter periods of time, the characterization of maximum variability of the temperature (and sound speed field) at mid-depth within the shelfbreak front during summer is robust.

7. Discussion

The primary goal of this study was to examine a well-sampled region to determine whether or not regional "hotspots" of uncertainty could be quantified and geographically identified. Using an improved climatology of the continental shelf and slope in the Middle Atlantic Bight, the shelfbreak region was identified as an area of enhanced variability (and thus uncertainty). Seasonal

attributes, including the sub-surface maximum in the standard deviation of the sound speed field during summer, were also determined. During spring off New Jersey, the near-surface layer over the continental shelf was also a region with a large standard deviation, comparable to the shelfbreak front. This is due to the presence of buoyant estuarine plumes from the Hudson River, and Delaware and Chesapeake Bays.

The climatology is useful for identifying regions of expected maxima in uncertainty in sound speed due to mesoscale and low-frequency phenomena. This is a prerequisite for understanding the much more complicated problem of uncertainty in transmission loss, which also includes issues relating to ocean bottom characteristics, high-frequency motions (particularly non-linear internal waves), and surface waves and surface roughness. Other studies in this volume consider the uncertainty in transmission loss from the Shelfbreak PRIMER experiment (Lermusieax, pers. comm.) In regions of the greatest variability and uncertainty of the sound speed, numerous important processes affect the propagation of sound, including reflection off the shelfbreak front (Lynch et al., 2003), presence of internal waves within the front (Duda, 2004), and mode scattering from internal waves (Sperry et al., 2004). Thus, although the climatology of sound speed does not address the magnitude of the effects of these different physical processes on transmission loss fluctuation, the regions of maximum sound speed variability are coincident with other effects which are geographically localized and impact transmission loss.

Despite the many limitations, the present climatology offers some very practical advantages. The climatology is relatively easy to produce, although clearly the availability of data varies greatly around the world. Examination of both the plan view fields of the standard deviation of the sound speed field offers a relatively simple and easily communicated means of identifying and prioritizing "hotspots" of mesoscale uncertainty. Finally, the identification of the peaks in variability and uncertainty in sound speed with an oceanographic feature, the shelfbreak front, provides a firm basis for further study focusing on uncertainty from both an oceanographic and acoustic perspective.

Acknowledgements

This work was supported under ONR Grant N00014-01-1-0772. The authors thank the program leader, Ellen Livingstone, for her leadership in this initiative. Numerous discussions with UNITES team members, including J. Lynch, P. Abbot, and P. Lermusieax, improved the manuscript. We also gratefully appreciate the efforts of P. Abbot in leading UNITES team efforts for the past three years.

References

Beardsley, R. C., D. C. Chapman, K. H. Brink, S. R. Ramp, and R. Schlitz, The Nantucket Shoals Flux Experiment (NSFE79) Part I: A basic description of the current and temperature variability, *Journal of Physical Oceanography*, *15*(6), 713-748, 1985.

Beardsley, R. C., S. J. Lentz, R. A. Weller, R. Limeburner, J. D. Irish, and J. B. Edson, Surface forcing on the southern flank of Georges Bank, February-August 1995, *J. Geophys. Res.*, *108*(C11), 8007, doi:10.1029/2002JC001359, 2003.

Biscaye, P. E., C. N. Flagg, and P. G. Falkowski. The Shelf Edge Exhange Processes Experiment, SEEP-II: An introduction to hypotheses, results, and conclusions, *Deep Sea Res., Part II, 41*, 231-252, 1994.

Bogden, P. S. and J. O'Donnell, Generalized Inverse analysis of current measurements from a moving ship: estimating the tidal and non-tidal flows in Long Island Sound. *J. Marine Res., 56*, 989-1014, 1997.

Chiu, C.-S., S. R. Ramp, C. W. Miller, J. F. Lynch, T. F. Duda, and T.-Y. Tang, Acoustic intensity fluctuations induced by South China Sea internal tides and solitons, submitted to *IEEE J. of Oceanic Engineering*, 2004.

Curry, R. G. *Hydrobase2: A Database of Hydrographic Profiles and Tools for Climatological Analysis* <http://www.whoi.edu/science/PO/hydrobase> (WHOI, 2002).

Duda, T. F., Acoustic mode coupling by nonlinear internal wave packets in a shelfbreak front area, *IEEE J. Oceanic Eng., 29*, 118-125, 2004.

Duda, T. F., and J. C. Preisig, A modeling study of acoustic propagation through moving shallow-water solitary wave packets, *IEEE J. Oceanic Eng., 24*, 16-32, 1999.

Gawarkiewicz, G. Linear stability models of shelfbreak fronts. *Journal of Physical Oceanography*, *21*(4), 471-48, 1991.

Gawarkiewicz, G., F. Bahr, K. H. Brink, R. C. Beardsley, M. Caruso, J. F. Lynch, and C.-S. Chiu. A large-amplitude meander of the shelfbreak front in the Middle Atlantic Bight: Observations from the Shelfbreak PRIMER Experiment. *J. Geophys. Res.*, *109*, doi:10.1029/2002JC001468, 2004.

Halliwell, G., and C. Mooers, The space-time structure and variability of the shelf-slope water and Gulf Stream surface temperature fronts and associated warm-core eddies, *J. Geophys. Res.*, *84*(C12), 7,707-7,725, 1979.

Houghton, R. W., R. Schlitz, R. C. Beardsley, B. Butman, and J. L. Chamberlin, The Middle Atlantic Bight cold pool: evolution of the temperature structure during summer 1979, *Journal of Physical Oceanography*, *12*, 1019-1029, 1982.

Lentz, S., K. Shearman, S. Anderson, A. Plueddemann, and J. Edson. Evolution of stratification over the New England shelf during the Coastal Mixing and Optics study, August 1996–June 1997. *J. Geophys. Res*., *108*(C1), doi:10.1029/2001JC001121, 2003.

Levitus, S., T. P. Boyer, M. E. Conkright, T. O'Brien, J. Antonov, C. Stephens, L. Stathoplos, D. Johnson, R. Gelfeld, *NOAA Atlas NESDIS 18, World Ocean Database 1998: Volume 1: Introduction*, U.S. Gov. Printing Office, Wash., D.C., 346 pp., 1998.

Linder, C. A. and G. Gawarkiewicz, A climatology of the shelfbreak front in the Middle Atlantic Bight, *J. Geophys. Res*., *103*, 18,405-18,423, 1998.

Lozier, M. S., M. S. Reed, and G. Gawarkiewicz, Instability of a Shelfbreak Front. *Journal of Physical Oceanography, 32*, 924-944, 2002.

Lynch, J. F., Newhall, A., Sperry, B., Gawarkiewicz, G., Fredricks, A., Tyack, P., Chiu, C. S., and P. Abbot. Spatial and temporal variations in acoustic propagation characteristics at the New England shelfbreak front. *IEEE J. Oceanic Engineering*, *28*, 129-150, 2003.

Mountain, D. G., Variability in the properties of Shelf Water in the Middle Atlantic Bight, 1977-1999, *J. Geophys. Res.*, *108*(C1), 3014, doi:10.1029/2001JC001044, 2003.

Naimie, C. E., J. W. Loder, and D. R. Lynch, Seasonal variation of the three-dimensional residual circulation on Georges Bank, *J. Geophys. Res*., *99*, 15,967-15,990, 1994.

Sperry, B., J. Lynch, G. Gawarkiewicz, C.-S. Chiu, and A. Newhall, Characteristics of acoustic propagation to the eastern vertical line array receiver during the summer 1996 New England Shelfbreak PRIMER experiment, in press, *IEEE J. of Oceanic Engineering*, 2004.

Wright, W. R., The limits of shelf water south of Cape Cod, 1941 to 1972, *Journal of Marine Research, 34*(1), 1-14, 1976.

Wright, W. R. and C. E. Parker, A volumetric temperature/salinity census for the Middle Atlantic Bight, *Limnology and Oceanography, 21*, 563-571, 1976.

Zhou, J. X., Z. X. Zhang, and P. Rogers, Resonant interaction of sound waves with internal solitons in the coastal zone, *J. Acoust. Soc. Am., 90*, 2042-2054, 1991.

Figure Captions

Figure 1: The Middle Atlantic Bight. The spatial extent of data for the plan view means is represented by the shaded area. Nantucket Shoals and New Jersey study areas denoted by boxes. Bathymetry contoured in meters.

Figure 2: (a) Sample plot of gridpoints, showing the 25km range rings for two adjacent grid nodes. (b) Hamming window weighting function.

Figure 3: Number of observations per grid point for (a) Winter, (b) Spring, (c) Summer, and (d) Fall.

Figure 4: Mid-depth (40-55m) mean temperature (°C) for (a) Winter, (b) Spring, (c) Summer, and (d) Fall.

Figure 5: Mid-depth (40-55m) mean salinity for (a) Winter, (b) Spring, (c) Summer, and (d) Fall.

Figure 6: Mid-depth (40-55m) salinity standard deviation for (a) Winter, (b) Spring, (c) Summer, and (d) Fall.

Figure 7: Mid-depth (40-55m) mean sound speed (m s^{-1}) for (a) Winter, (b) Spring, (c) Summer, and (d) Fall.

Figure 8: Mid-depth (40-55m) sound speed standard deviation (m s^{-1}) for (a) Winter, (b) Spring, (c) Summer, and (d) Fall.

Figure 9: Cross-shelf mean temperature (color, °C) overlaid with standard deviation for Nantucket Shoals for (a) Winter, (b) Spring, (c) Summer, and (d) Fall.

Figure 10: Cross-shelf mean salinity (color) overlaid with standard deviation for Nantucket Shoals for (a) Winter, (b) Spring, (c) Summer, and (d) Fall.

Figure 11: Cross-shelf mean sound speed (color, m s^{1}) overlaid with standard deviation for Nantucket Shoals for (a) Winter, (b) Spring, (c) Summer, and (d) Fall.

Figure 12: Cross-shelf mean temperature (color, °C) overlaid with standard deviation for New Jersey for (a) Winter, (b) Spring, (c) Summer, and (d) Fall.

Figure 13: Cross-shelf mean salinity (color) overlaid with standard deviation for New Jersey for (a) Winter, (b) Spring, (c) Summer, and (d) Fall.

Figure 14: Cross-shelf mean sound speed (color, m s^{-1}) overlaid with standard deviation for New Jersey for (a) Winter, (b) Spring, (c) Summer, and (d) Fall.

Figure 15: Histogram of temperature time series data from NSFE shelf mooring (thermistor at 32m depth, plots a-d) and slope mooring (28m depth, plots e-h).

Figure 16: Near-surface stratification shown by (a) Difference between temperature at 5m and 20m, (b) Maximum stratification, and (c) Location of maximum stratification. Raw data is shown as gray points, mean and standard deviation as darker lines.

Figure 17: The mean cross-shelf temperature from six cross-shelf sections taken from the Shelfbreak PRIMER experiment during July 26-31, 1996.

Figure 18: Amplitude of the first two empirical orthogonal functions for temperature from the six sections above. (a) The first mode, accounting for 43% of the variance, with a peak at

the offshore edge of the section, where the shelfbreak front intersects the seasonal pycnocline. (b) The second mode accounting for 27% of the variance.

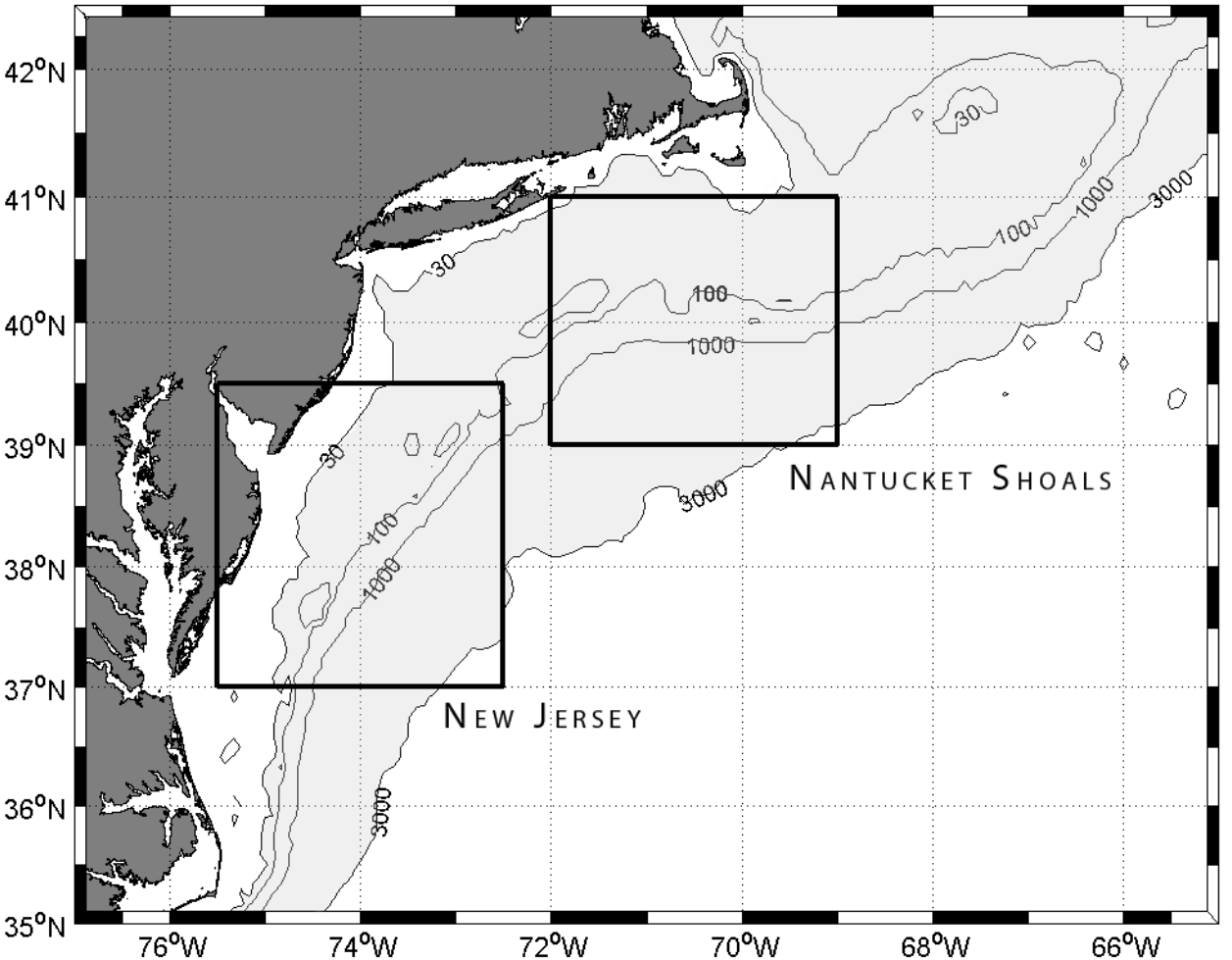
42°N
41°N
40°N
39°N
38°N
37°N
36°N
35°N
76°W
74°W
72°W
70°W
68°W
66°W
30
100
1000
3000
NANTUCKET SHOALS
NEW JERSEY

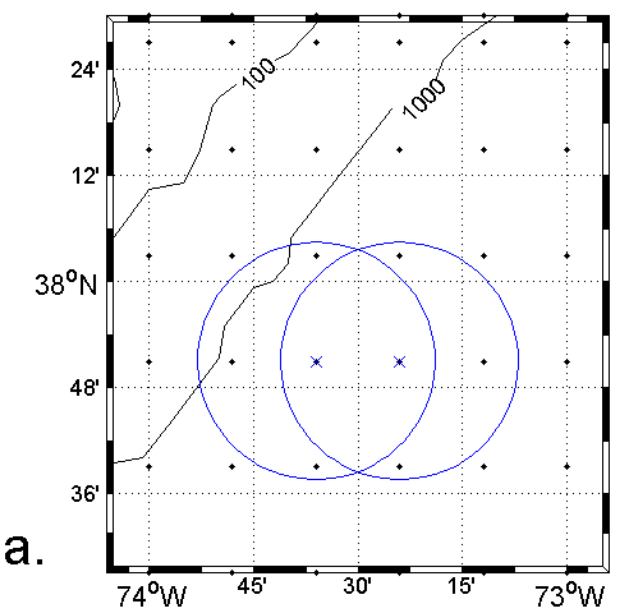
100
1000
24'
12'
38°N
48'
36'
74°W
45'
30'
15'
73°W

a.

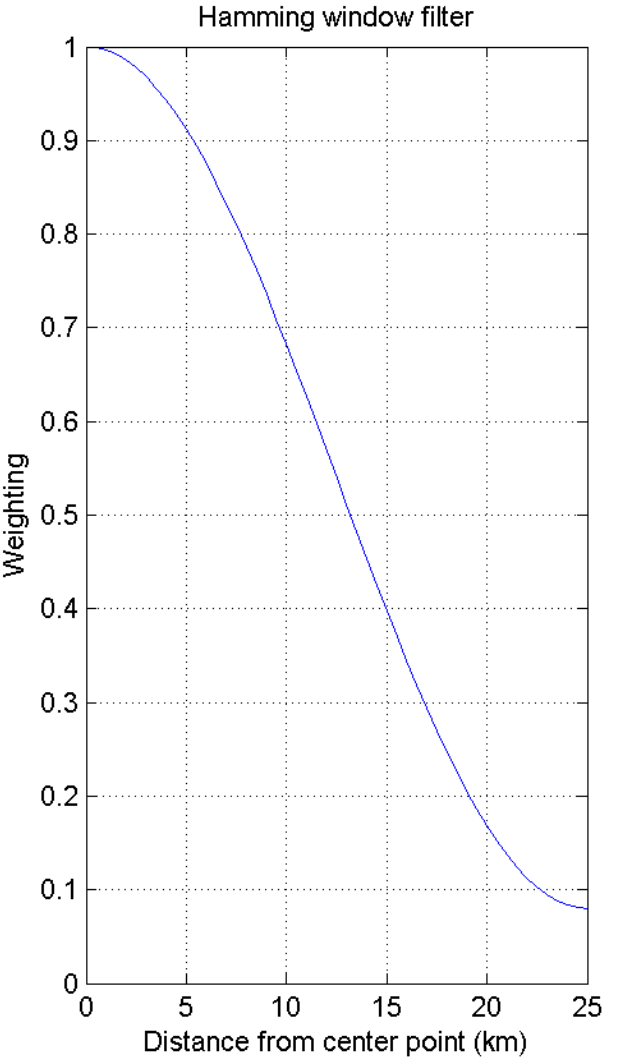
Hamming window filter
Weighting
Distance from center point (km)
0
0.1
0.2
0.3
0.4
0.5
0.6
0.7
0.8
0.9
1
0
5
10
15
20
25

b.

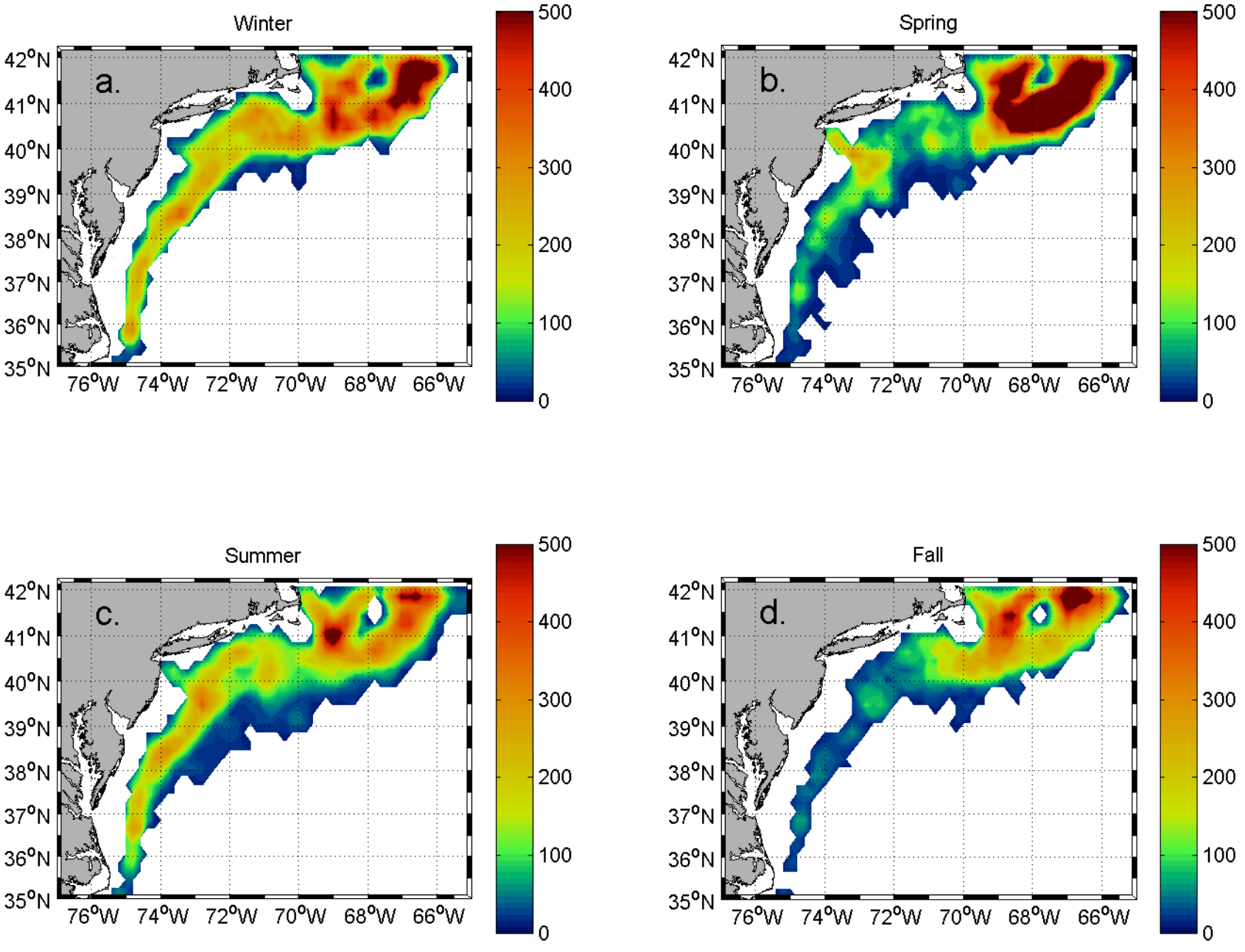
Winter
a.
Spring
b.
Summer
c.
Fall
d.
42°N
41°N
40°N
39°N
38°N
37°N
36°N
35°N
76°W
74°W
72°W
70°W
68°W
66°W
500
400
300
200
100
0

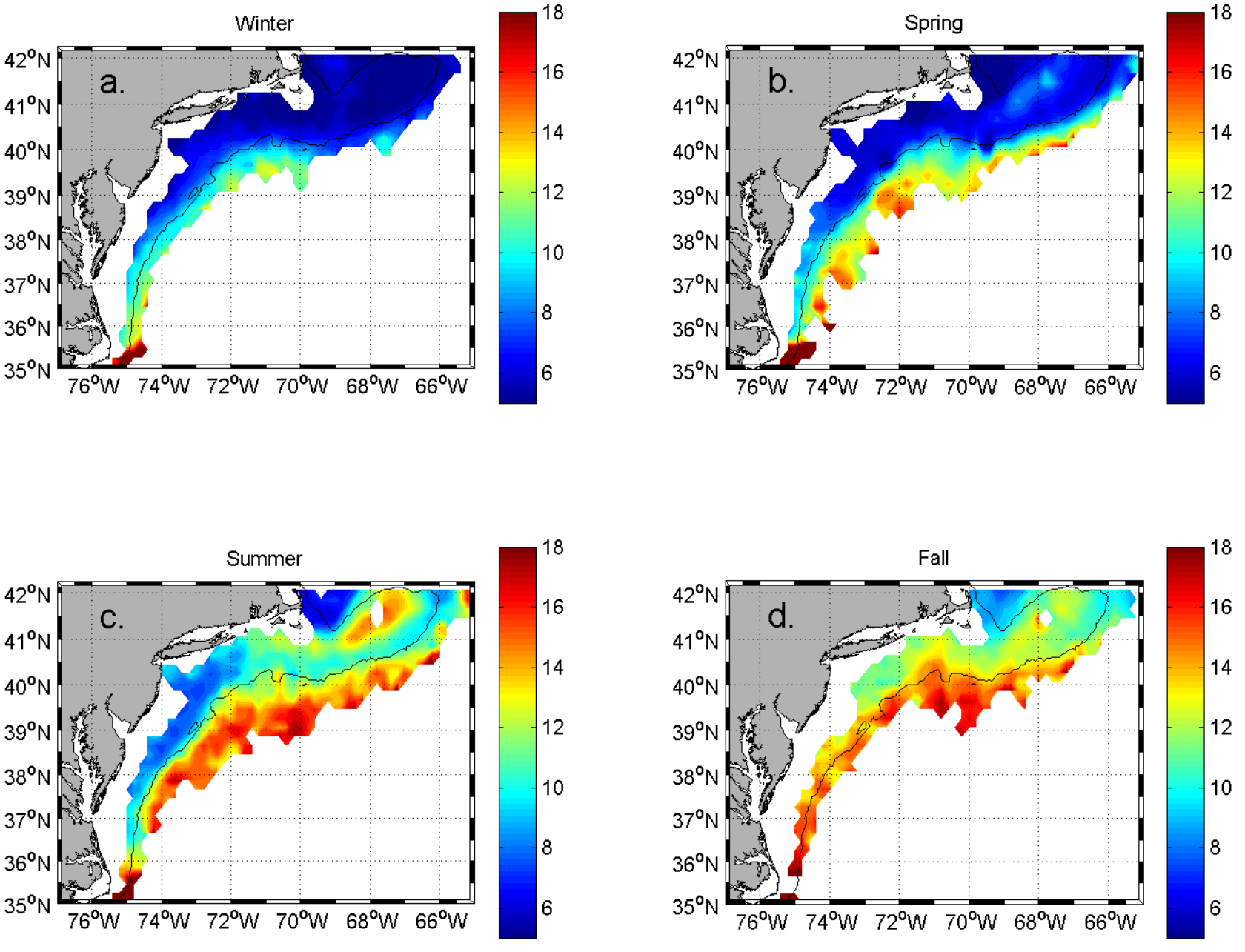
Winter
a.
Spring
b.
Summer
c.
Fall
d.
42°N
41°N
40°N
39°N
38°N
37°N
36°N
35°N
76°W
74°W
72°W
70°W
68°W
66°W
18
16
14
12
10
8
6

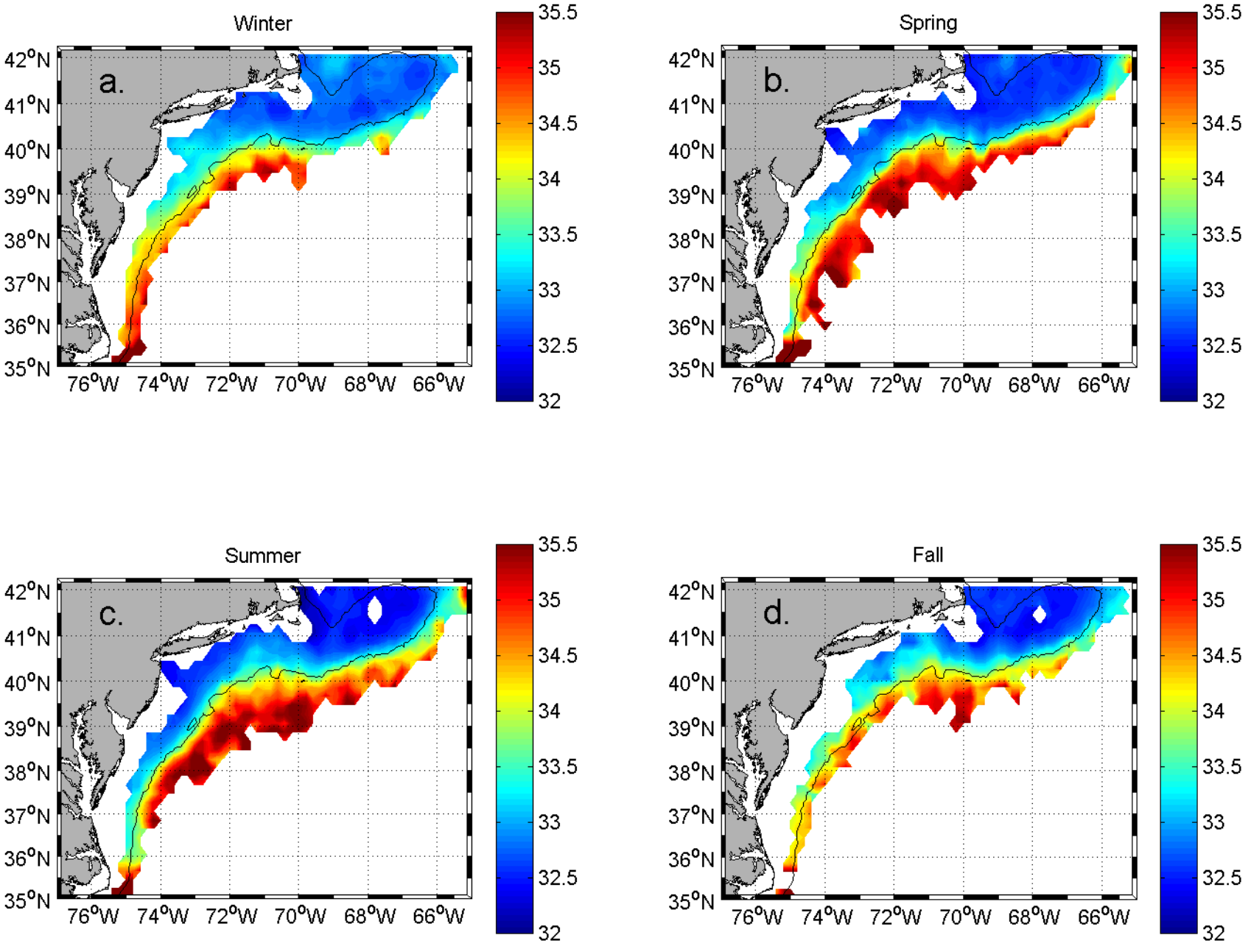
Winter
a.
Spring
b.
Summer
c.
Fall
d.
42°N
41°N
40°N
39°N
38°N
37°N
36°N
35°N
76°W
74°W
72°W
70°W
68°W
66°W
35.5
35
34.5
34
33.5
33
32.5
32

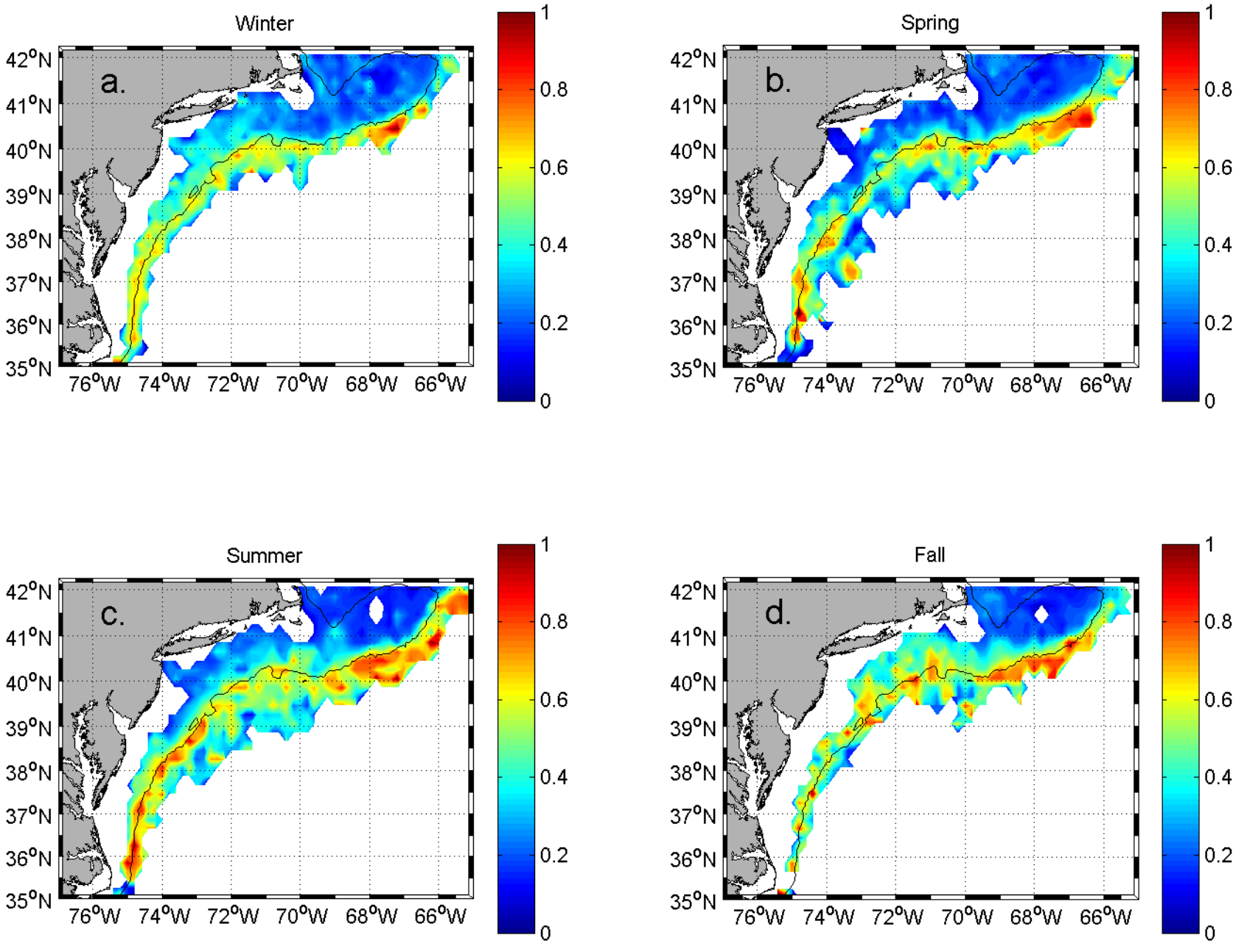
Winter
a.
Spring
b.
Summer
c.
Fall
d.
42°N
41°N
40°N
39°N
38°N
37°N
36°N
35°N
76°W
74°W
72°W
70°W
68°W
66°W
1
0.8
0.6
0.4
0.2
0

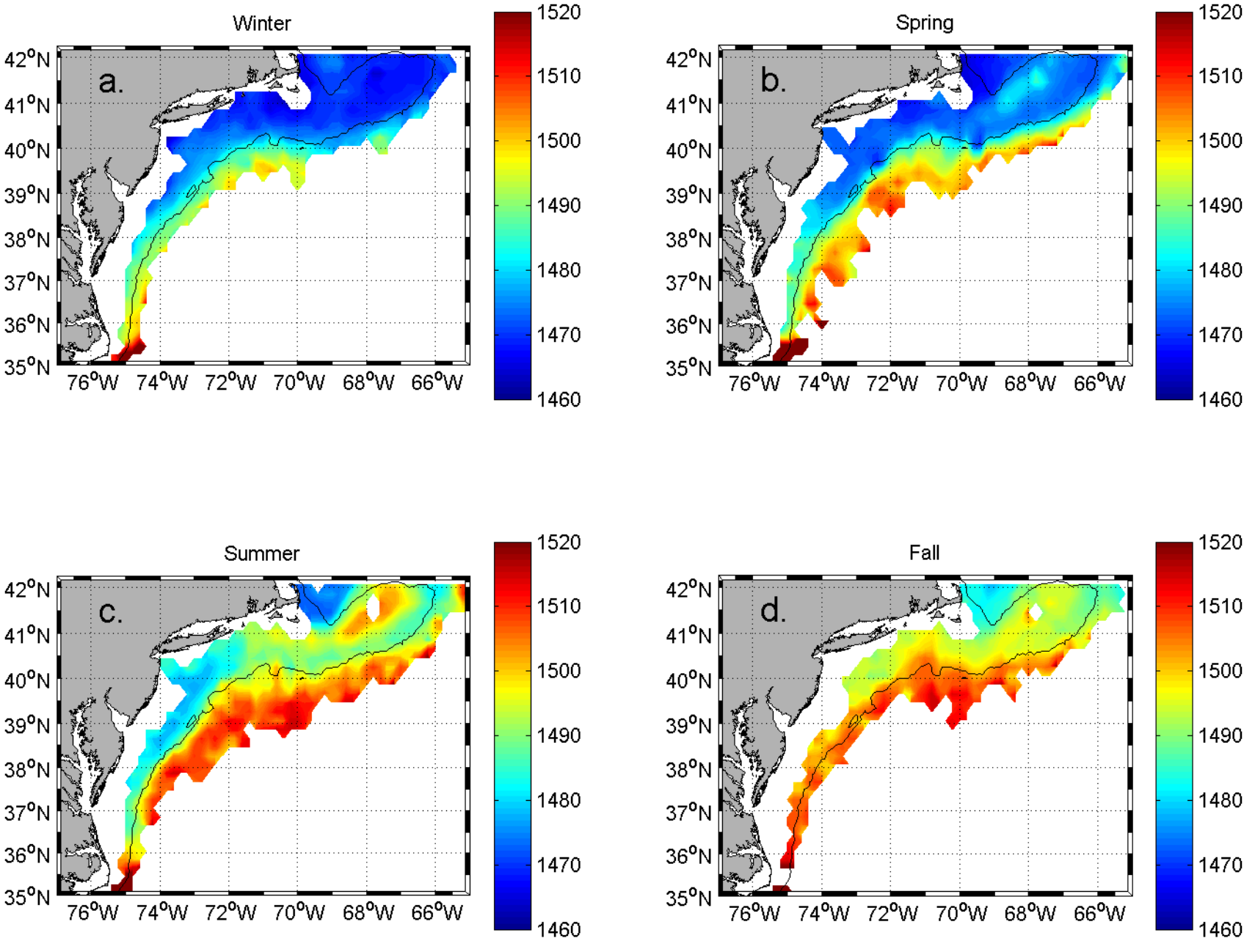
Winter
a.
Spring
b.
Summer
c.
Fall
d.
42°N
41°N
40°N
39°N
38°N
37°N
36°N
35°N
76°W
74°W
72°W
70°W
68°W
66°W
1520
1510
1500
1490
1480
1470
1460

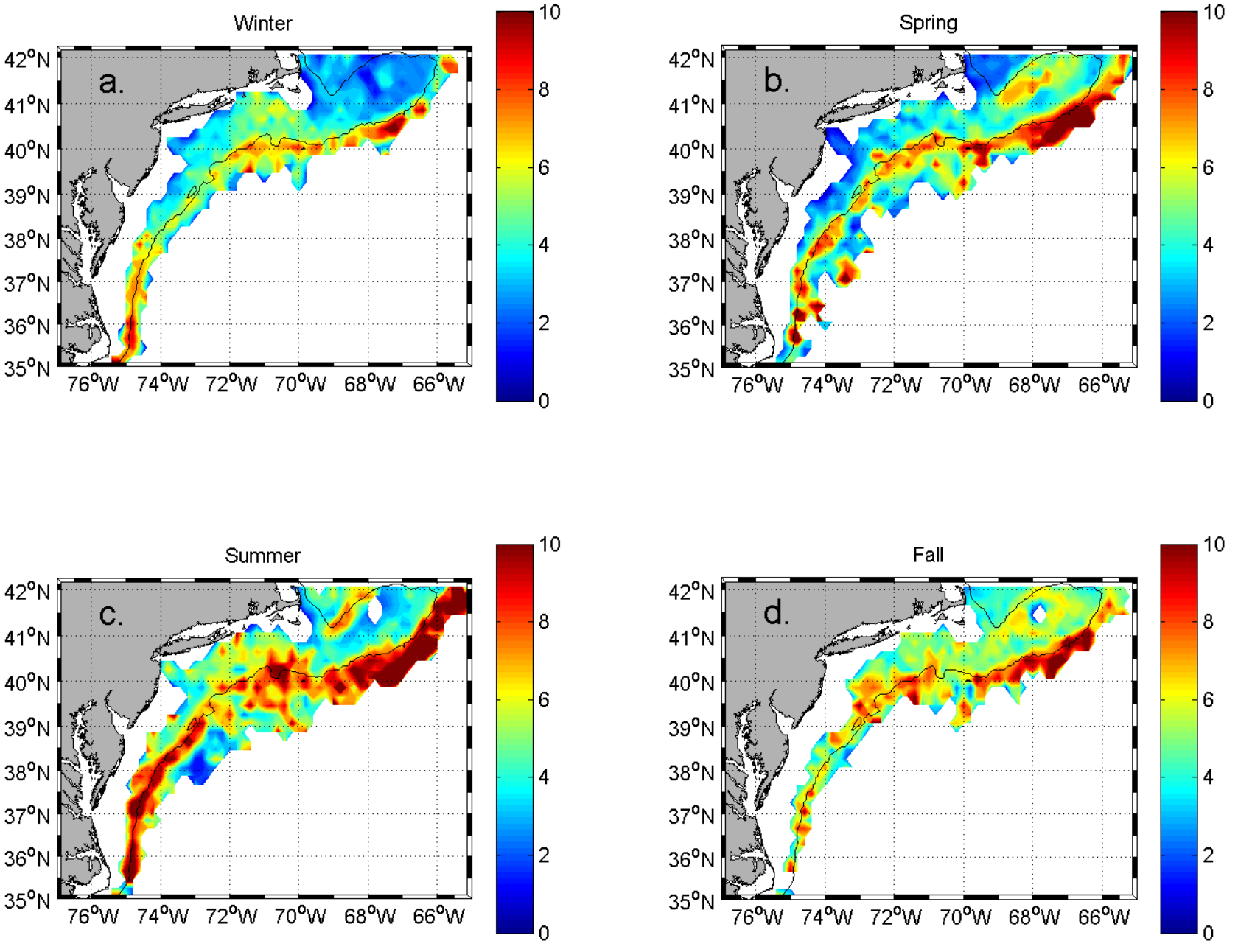
Winter
a.
Spring
b.
Summer
c.
Fall
d.
42°N
41°N
40°N
39°N
38°N
37°N
36°N
35°N
76°W
74°W
72°W
70°W
68°W
66°W
10
8
6
4
2
0

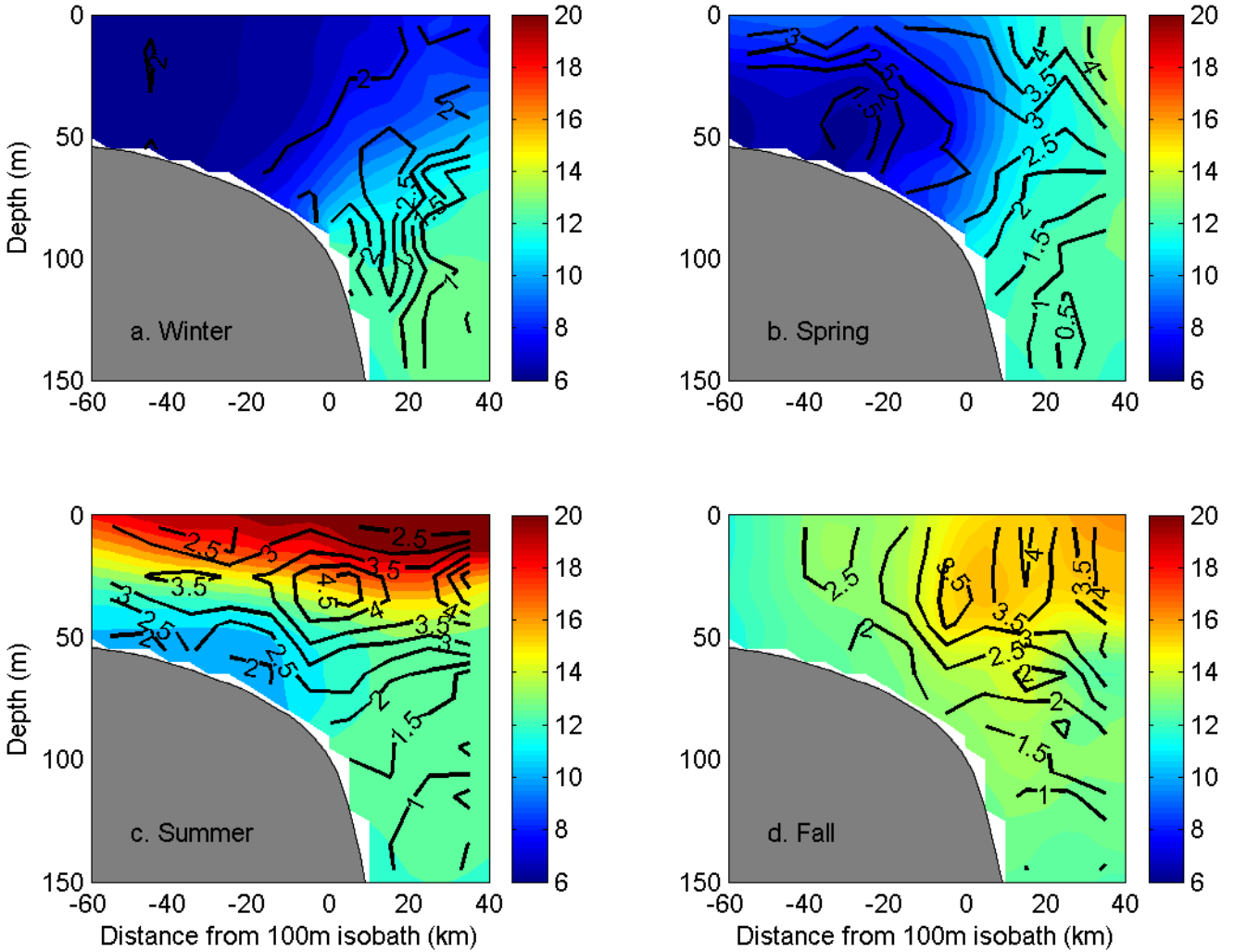
a. Winter
b. Spring
c. Summer
d. Fall
Depth (m)
Distance from 100m isobath (km)
0
50
100
150
-60
-40
-20
0
20
40
6
8
10
12
14
16
18
20

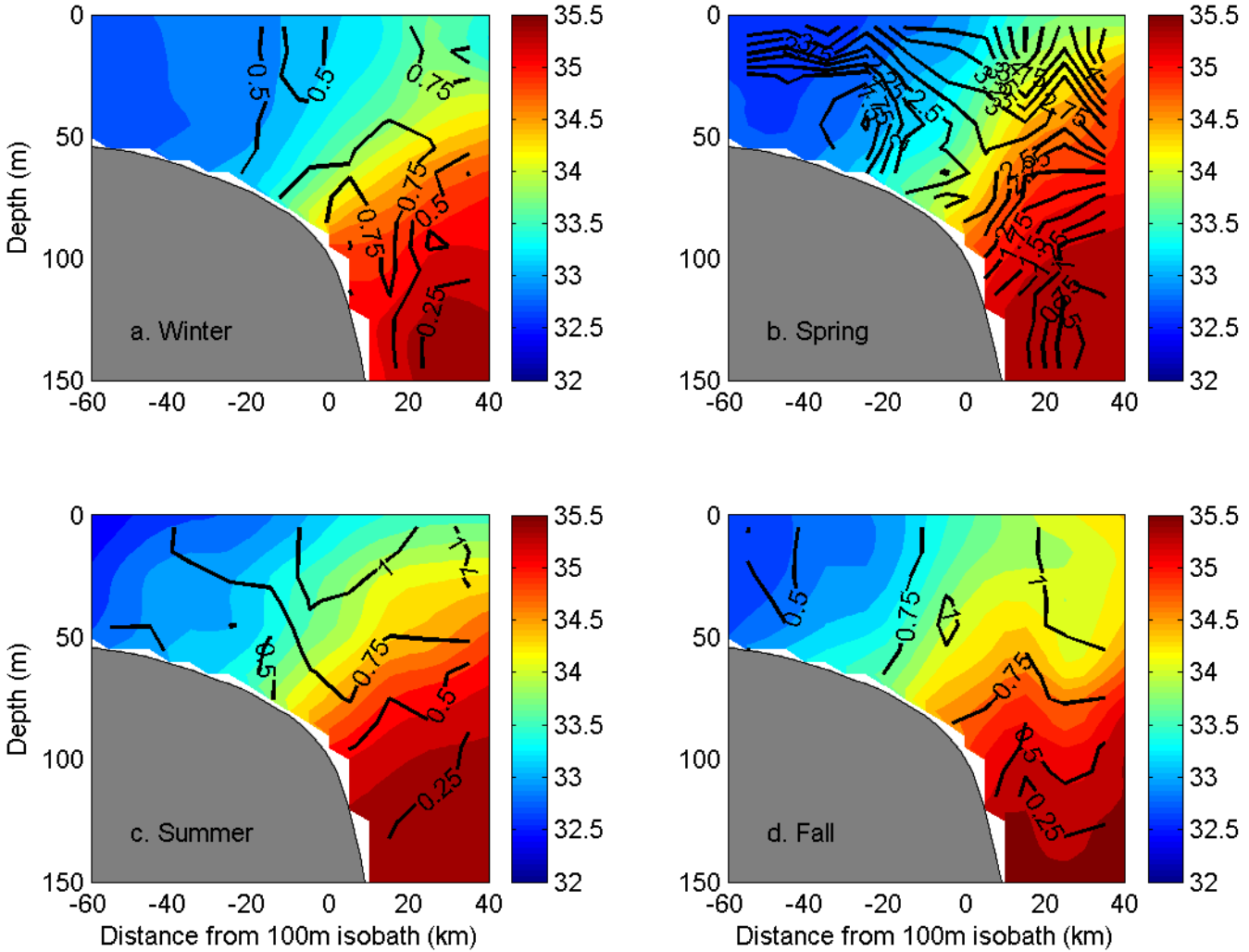
a. Winter
b. Spring
c. Summer
d. Fall
Depth (m)
Distance from 100m isobath (km)
0
50
100
150
-60
-40
-20
0
20
40
35.5
35
34.5
34
33.5
33
32.5
32

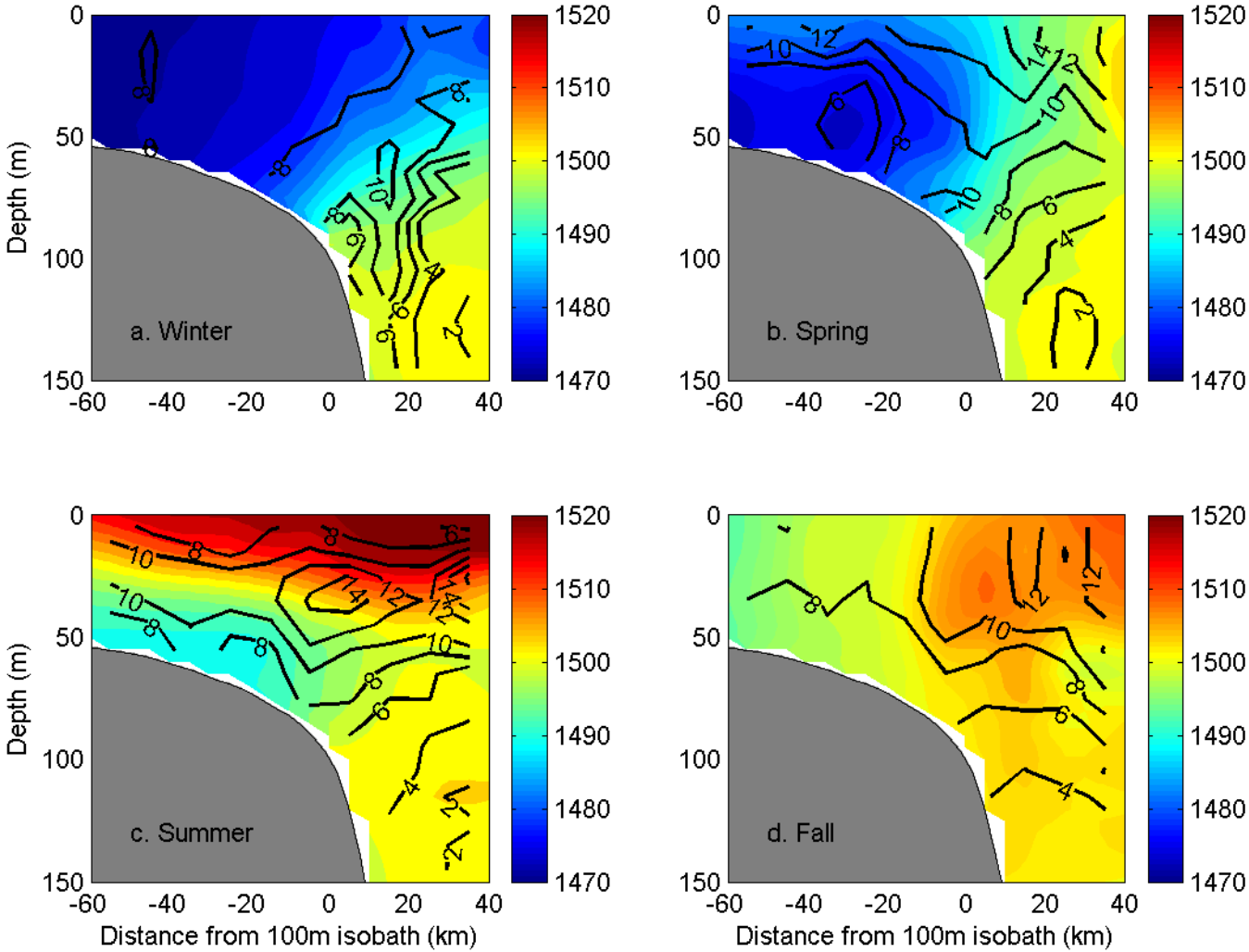
a. Winter
b. Spring
c. Summer
d. Fall
Depth (m)
Distance from 100m isobath (km)
0
50
100
150
-60
-40
-20
0
20
40
1520
1510
1500
1490
1480
1470

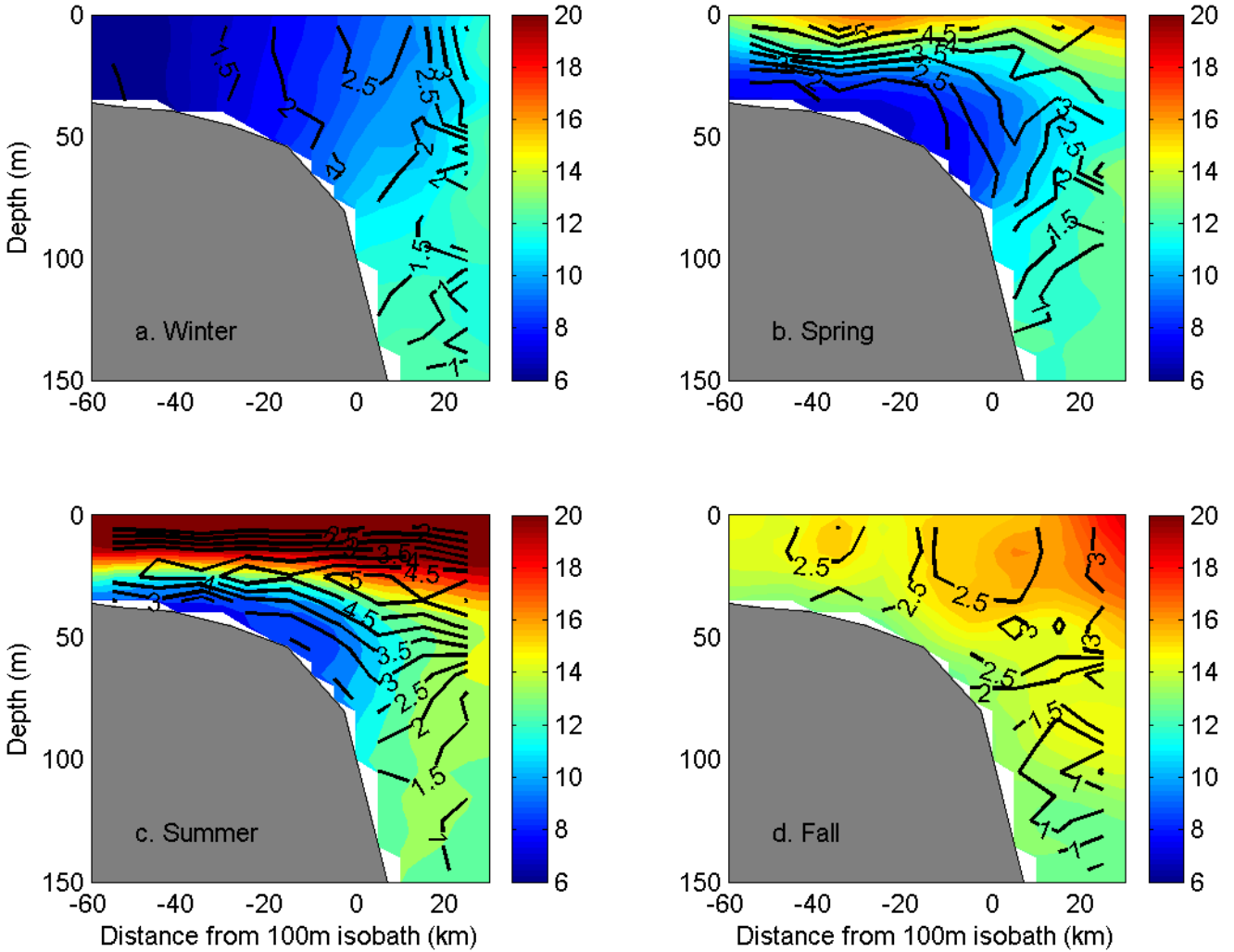
a. Winter
b. Spring
c. Summer
d. Fall
Depth (m)
Distance from 100m isobath (km)
0
50
100
150
-60
-40
-20
0
20
6
8
10
12
14
16
18
20

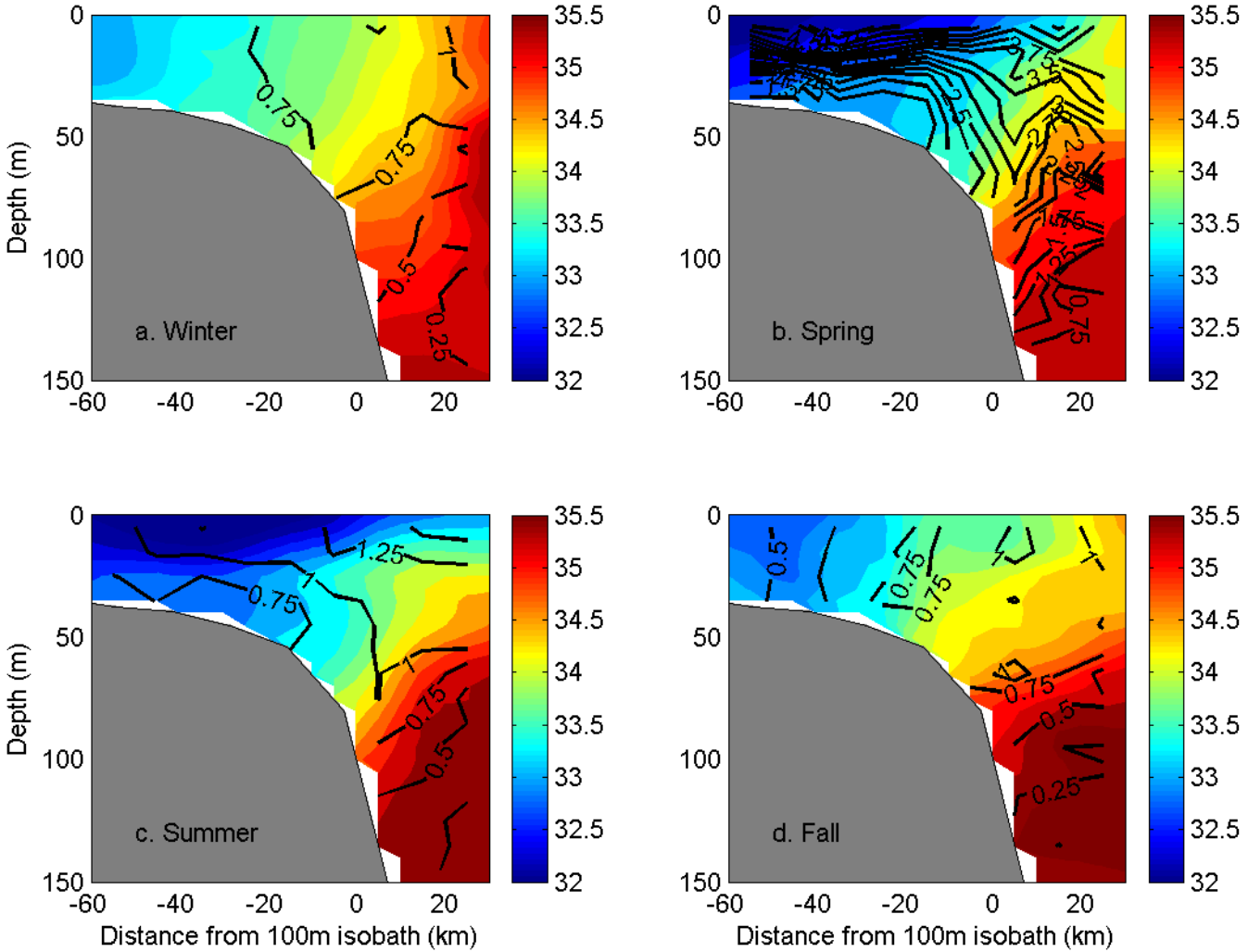
a. Winter
b. Spring
c. Summer
d. Fall
Depth (m)
Distance from 100m isobath (km)
0
50
100
150
-60
-40
-20
0
20
35.5
35
34.5
34
33.5
33
32.5
32

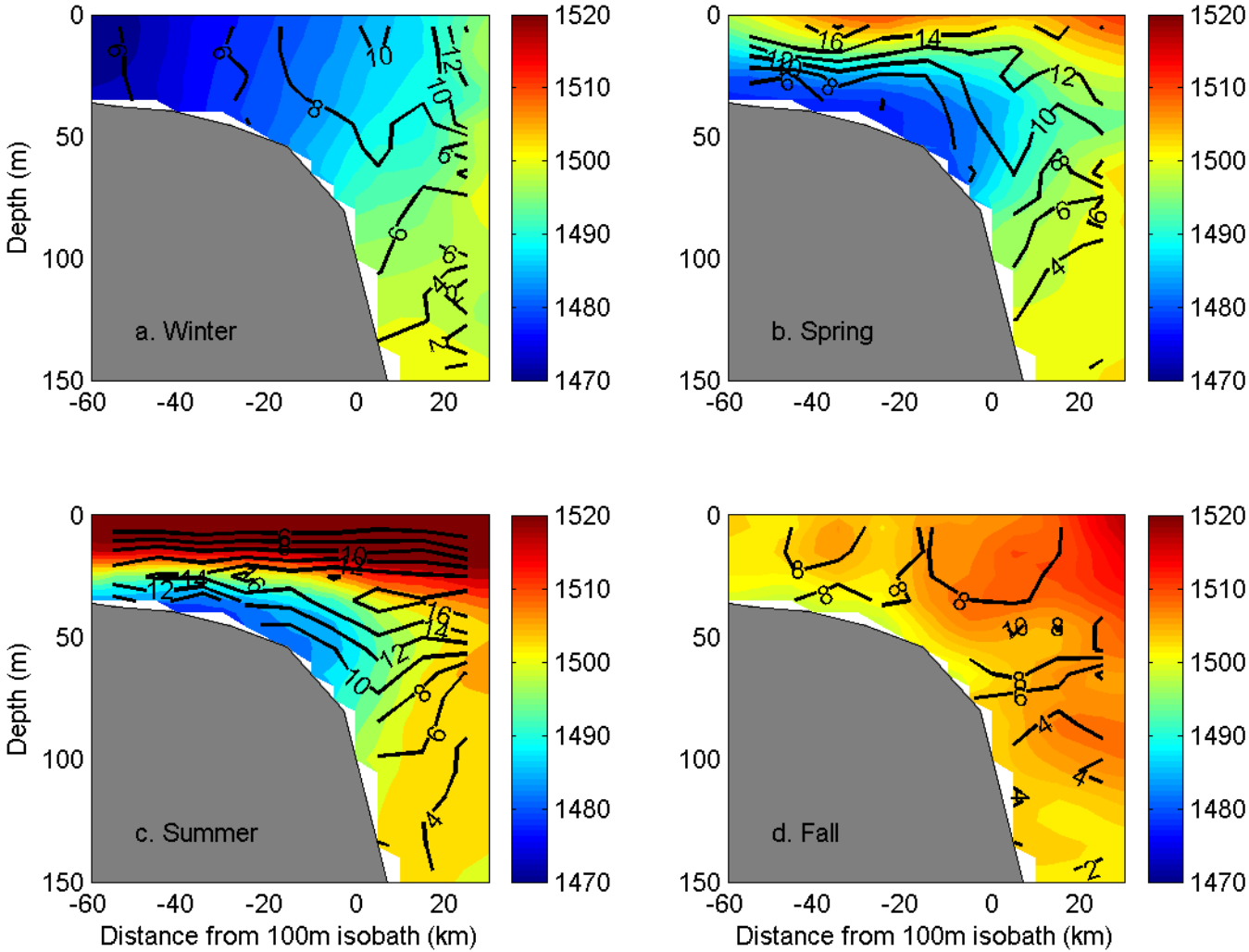
a. Winter
b. Spring
c. Summer
d. Fall
Depth (m)
Distance from 100m isobath (km)
0
50
100
150
-60
-40
-20
0
20
1520
1510
1500
1490
1480
1470

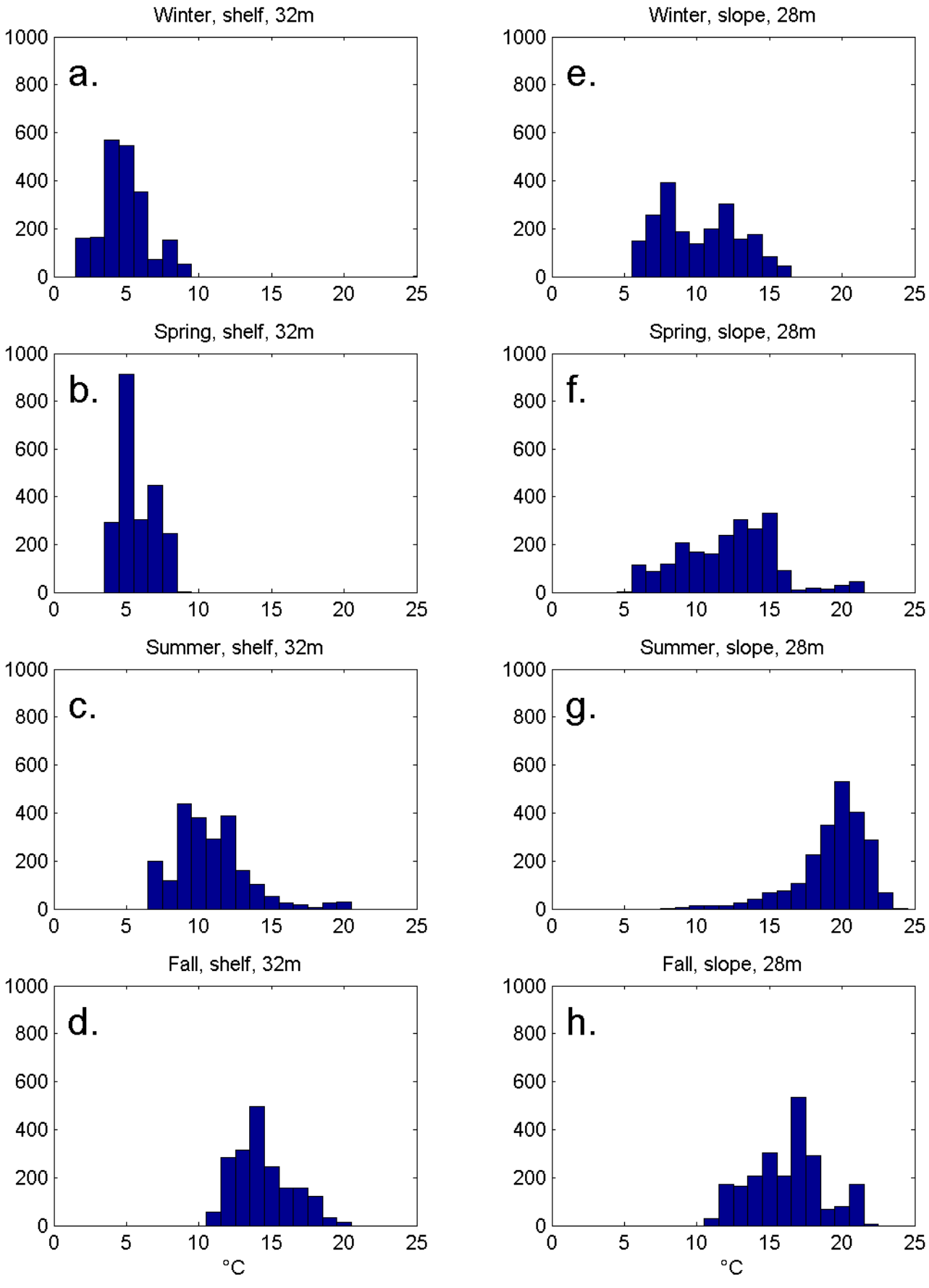
Winter, shelf, 32m
a.
Winter, slope, 28m
e.
Spring, shelf, 32m
b.
Spring, slope, 28m
f.
Summer, shelf, 32m
c.
Summer, slope, 28m
g.
Fall, shelf, 32m
d.
Fall, slope, 28m
h.
0
200
400
600
800
1000
0
5
10
15
20
25
°C

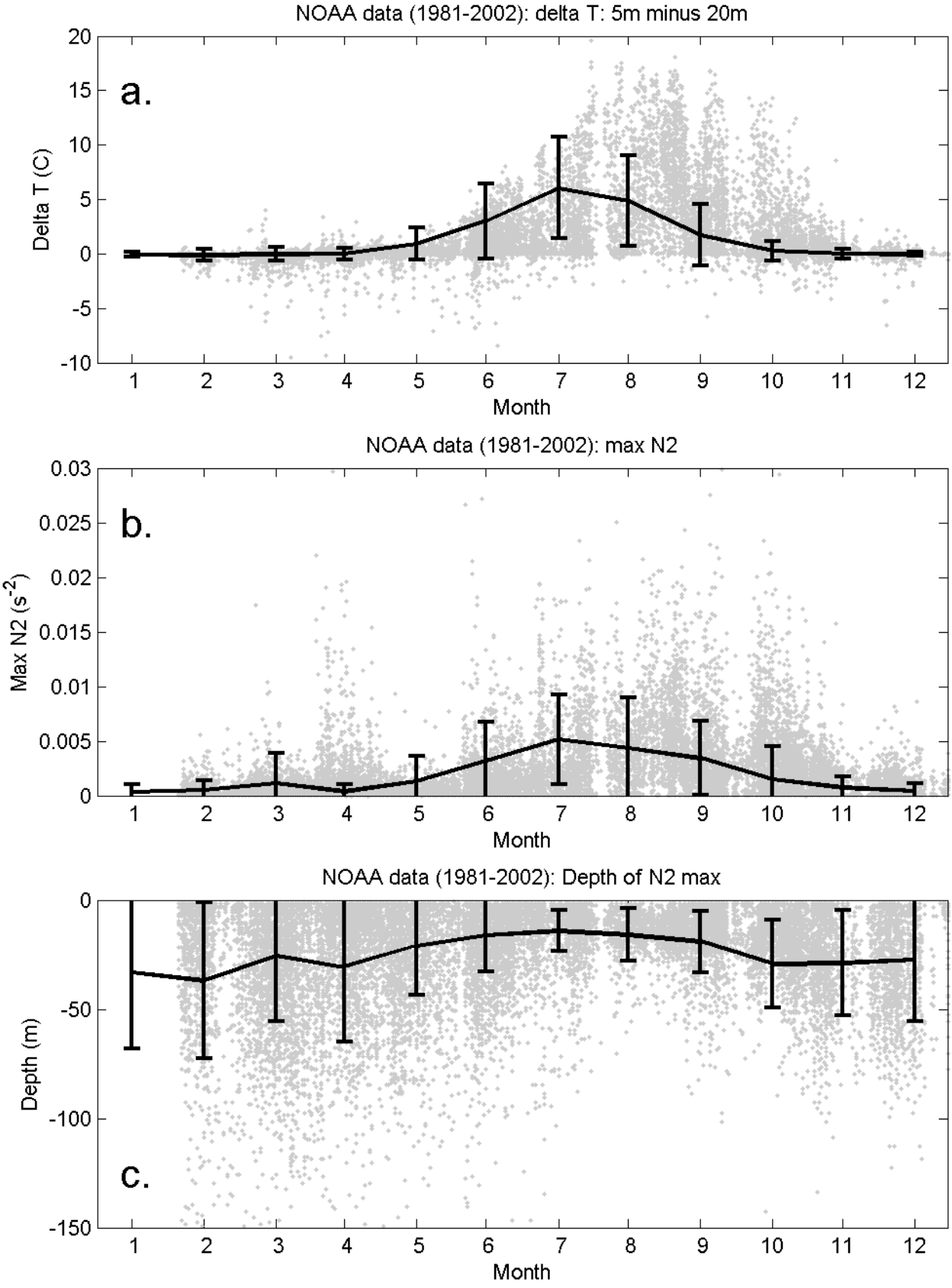
NOAA data (1981-2002): delta T: 5m minus 20m
a.
Delta T (C)
20
15
10
5
0
-5
-10
1
2
3
4
5
6
7
8
9
10
11
12
Month
NOAA data (1981-2002): max N2
b.
Max N2 (s-2)
0.03
0.025
0.02
0.015
0.01
0.005
0
Month
NOAA data (1981-2002): Depth of N2 max
c.
Depth (m)
0
-50
-100
-150
Month

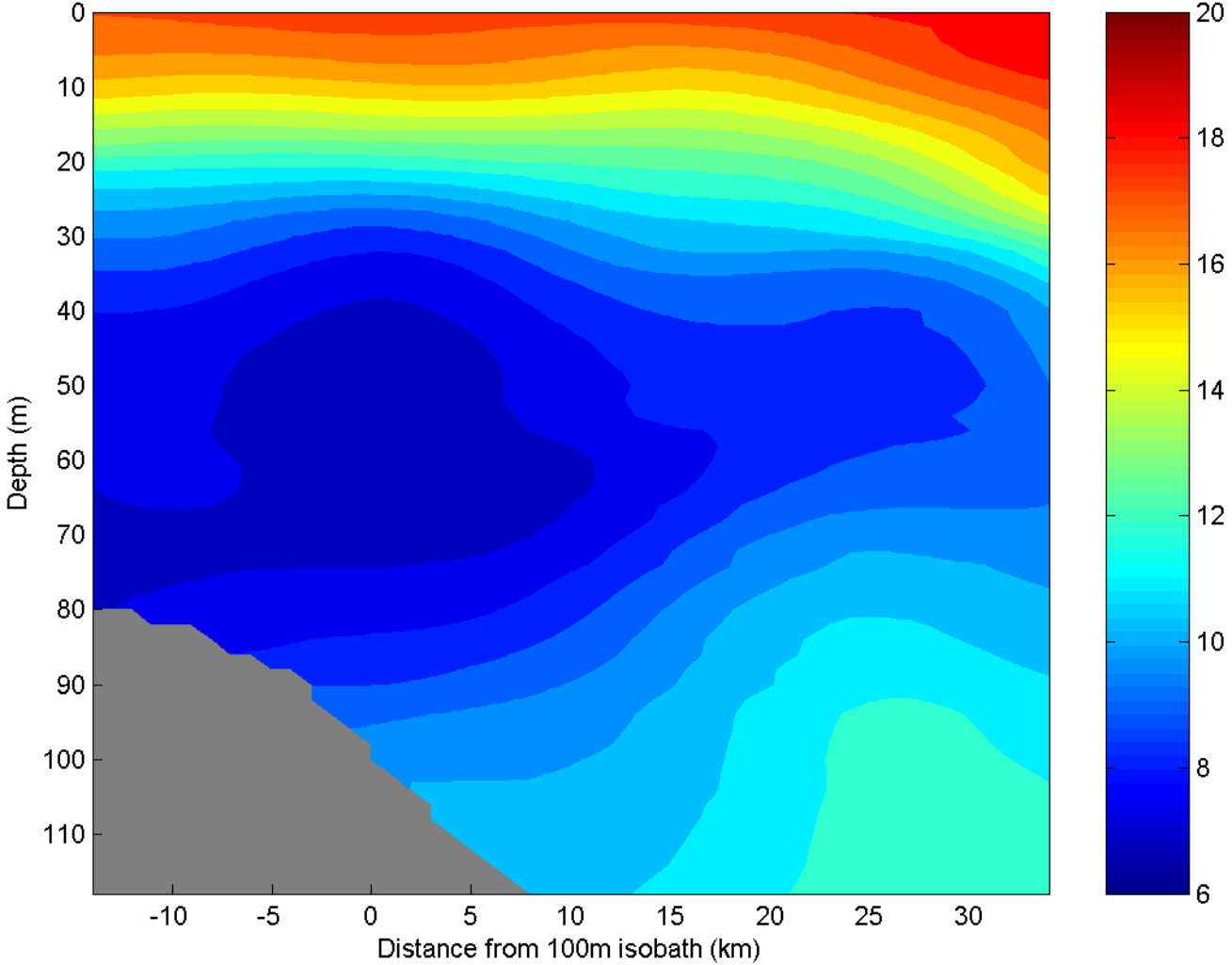
0
10
20
30
40
50
60
70
80
90
100
110
Depth (m)
-10
-5
0
5
10
15
20
25
30
Distance from 100m isobath (km)
20
18
16
14
12
10
8
6

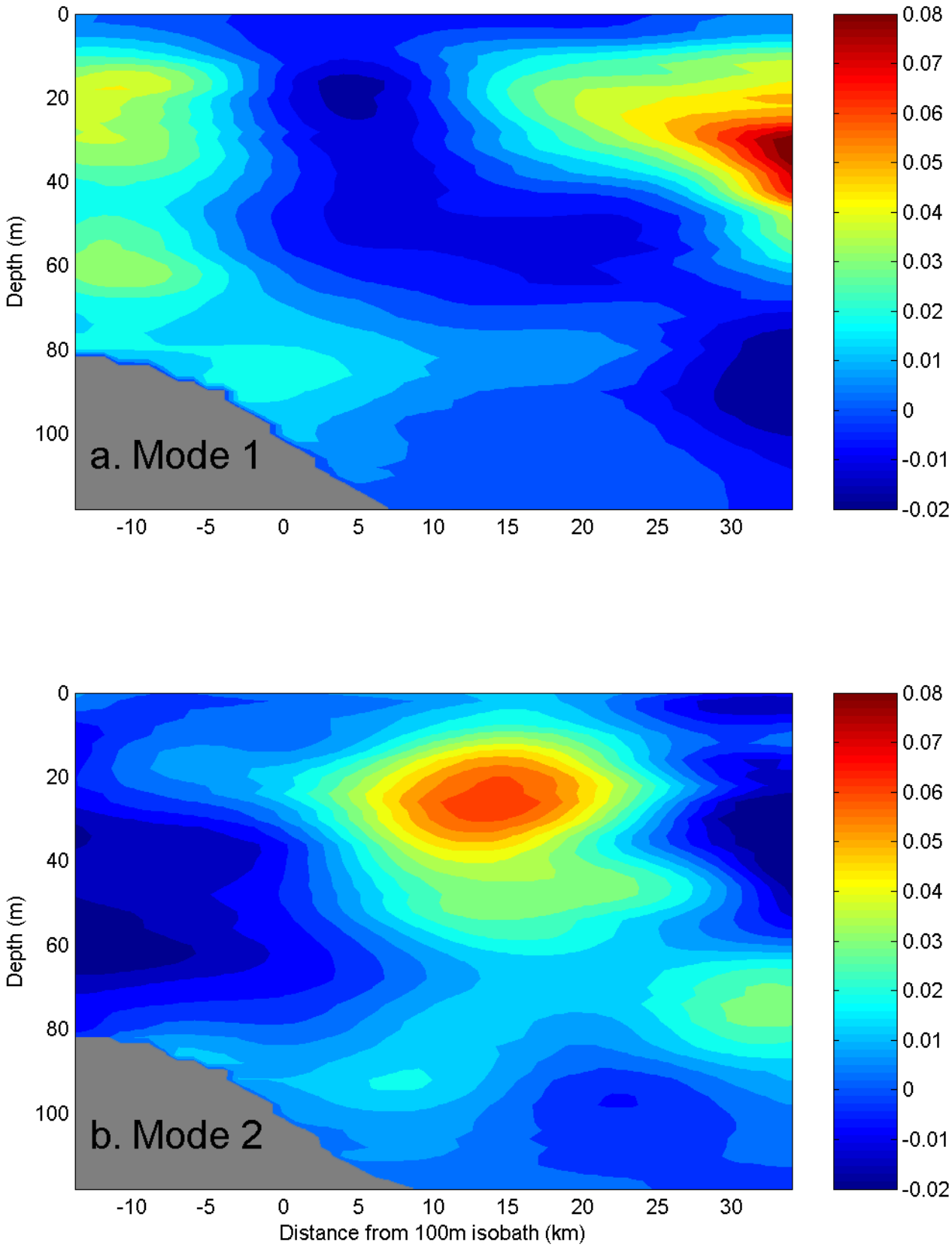
0
20
40
60
80
100
Depth (m)
a. Mode 1
-10
-5
0
5
10
15
20
25
30
0.08
0.07
0.06
0.05
0.04
0.03
0.02
0.01
0
-0.01
-0.02
b. Mode 2
Distance from 100m isobath (km)